ERRγ agonist under mechanical stretching manifests hypertrophic cardiomyopathy phenotypes of engineered cardiac tissue through maturation

AUTHOR(S):

Fujiwara, Yuya; Miki, Kenji; Deguchi, Kohei; Naka, Yuki; Sasaki, Masako; Sakoda, Ayaka; Narita, Megumi; ... Nishimoto, Tomoyuki; Imahashi, Kenichi; Yoshida, Yoshinori

CITATION:

Fujiwara, Yuya ...[et al]. ERRγ agonist under mechanical stretching manifests hypertrophic cardiomyopathy phenotypes of engineered cardiac tissue through maturation. Stem Cell Reports 2023, 18(11): 2108-2122

ISSUE DATE:

2023-11-14

URL:

http://hdl.handle.net/2433/286048

Stem Cell Reports
Article
ISSCR
OPEN ACCESS

ERRγ agonist under mechanical stretching manifests hypertrophic cardiomyopathy phenotypes of engineered cardiac tissue through maturation

Yuya Fujiwara,[1,2] Kenji Miki,[1,3,4,9,*] Kohei Deguchi,[2,5] Yuki Naka,[1,2] Masako Sasaki,[1,2] Ayaka Sakoda,[2,5] Megumi Narita,[1] Sachiko Imaichi,[6,10] Tsukasa Sugo,[7] Shunsuke Funakoshi,[1,2] Tomoyuki Nishimoto,[8] Kenichi Imahashi,[2,5] and Yoshinori Yoshida[1,2,*]

[1]Center for iPS Cells Research and Application, Kyoto University, Kyoto, Japan
[2]Takeda-CiRA Joint Program, Fujisawa, Japan
[3]Center for Organ Engineering, Department of Surgery, Massachusetts General Hospital, Boston, MA, USA
[4]Department of Surgery, Harvard Medical School, Boston, MA, USA
[5]T-CiRA Discovery, Takeda Pharmaceutical Company Limited, Fujisawa, Japan
[6]Pharmaceutical Science, Takeda Pharmaceutical Company Limited, Fujisawa, Japan
[7]GenAhead Bio Inc., Fujisawa, Japan
[8]Orizuru therapeutic Inc., Fujisawa, Japan
[9]Present address: Premium Research Institute for Human Metaverse Medicine, Osaka University, Suita, Japan
[10]Present address: Department of Molecular Biology, Massachusetts General Hospital, Boston, MA 02114, USA
*Correspondence: kenjimiki.prime@osaka-u.ac.jp (K.M.), yoshinor@cira.kyoto-u.ac.jp (Y.Y.)
https://doi.org/10.1016/j.stemcr.2023.09.003

SUMMARY

Engineered cardiac tissue (ECT) using human induced pluripotent stem cell-derived cardiomyocytes is a promising tool for modeling heart disease. However, tissue immaturity makes robust disease modeling difficult. Here, we established a method for modeling hypertrophic cardiomyopathy (HCM) malignant (MYH7 R719Q) and nonmalignant (MYBPC3 G115*) pathogenic sarcomere gene mutations by accelerating ECT maturation using an ERRγ agonist, T112, and mechanical stretching. ECTs treated with T112 under 10% elongation stimulation exhibited more organized and mature characteristics. Whereas matured ECTs with the MYH7 R719Q mutation showed broad HCM phenotypes, including hypertrophy, hypercontraction, diastolic dysfunction, myofibril misalignment, fibrotic change, and glycolytic activation, matured MYBPC3 G115* ECTs displayed limited phenotypes, which were primarily observed only under our new maturation protocol (i.e., hypertrophy). Altogether, ERRγ activation combined with mechanical stimulation enhanced ECT maturation, leading to a more accurate manifestation of HCM phenotypes, including non-cardiomyocyte activation, consistent with clinical observations.

Yoshida and colleagues established a maturation method of engineered cardiac tissue (ECT) via ERRγ stimulation and mechanical stretching for hypertrophic cardiomyopathy (HCM) modeling. The combined approach effectively promoted ECT maturation, allowing HCM phenotypes to manifest to a greater extent, including non-cardiomyocyte changes such as fibrosis, to contrast more clearly the distinct disease phenotypes between malignant and nonmalignant pathogenic sarcomere mutations.

INTRODUCTION

Hypertrophic cardiomyopathy (HCM) is a disease characterized by hypertrophy of the left ventricle (Authors/Task Force members et al., 2014) and is estimated to affect 1 in 500 people (Maron et al., 1995). Approximately 60% of HCM cases are autosomal dominant genetic disorders of sarcomere components, and more than 1,400 HCM-associated mutations have been reported (Ho et al., 2015). About 70% of pathogenic HCM mutations are in the genes encoding myosin heavy chain β (*MYH7*) or myosin-binding protein C (*MyBPC3*) (Ho et al., 2015). Although much is known about the genetic basis of HCM, there are no established medical therapies for HCM other than symptomatic treatments. Since HCM disease models are extremely challenging to establish, the development of therapeutic agents for HCM treatment has been slower than desired.

Animal models have been used as platforms for HCM research to understand the underlying mechanism and develop novel therapeutics (Mosqueira et al., 2019). However, there are many interspecies differences between humans and other animals (Milani-Nejad and Janssen, 2014). Importantly, unlike in humans, the expression of *MYH7*, the most frequently mutated gene in HCM patients, is low in mice (Lompre et al., 1981), making it difficult to interpret the phenotypes of mouse HCM models. Therefore, establishing *in vitro* platforms to replicate human HCM phenotypes has great potential for biomedical applications.

Several studies have established two-dimensional (2D) HCM disease models using human induced pluripotent stem cell-derived cardiomyocytes (hiPSC-CMs) (Lan et al., 2013; Seeger et al., 2019), but they lack many critical features of diseased heart tissues, including 3D tissue structures and interactions between cardiomyocytes and non-cardiomyocytes. Thus, it is challenging to recapitulate the

full range of abnormalities in cardiomyocytes and non-cardiomyocytes with such models.

Engineered cardiac tissue (ECT) using hiPSC-CMs is a promising tool to recapitulate the human heart and can be readily applied to study human heart diseases *in vitro* (Mosqueira et al., 2018). However, ECTs derived from hiPSC-CMs are immature compared to the adult heart. Unlike adult ventricular CMs, hiPSC-CMs have an irregular sarcomere structure, low mitochondrial content, and lack T-tubule structure (Karbassi et al., 2020). Several studies have addressed such issues by using electrical stimulation (Ronaldson-Bouchard et al., 2018) and mechanical stretching (Leonard et al., 2018; Ruan et al., 2016) to improve the immaturity of ECTs. However, these methods require a much longer maturation period (i.e., 2–3 weeks).

Furthermore, despite several reports demonstrating the utility of ECTs for *in vitro* HCM models (Cohn et al., 2019; Ma et al., 2018), establishing an HCM model with a similar degree of malignancy observed in human HCM cases remains a challenge. For example, although MYH7 R403Q$^{-/+}$ ECTs showed cardiomyocyte hypertrophy (Cohn et al., 2019), this phenotype has never been reported in isogenic ECTs with MYBPC3 mutations (Cohn et al., 2019; Ma et al., 2018). Additionally, functional changes in non-cardiomyocytes, such as fibrosis, and the phenotypic diversity arising from different pathogenic mutations have not been shown using such models.

We hypothesized that mature ECTs are required to model the full spectrum of HCM pathophysiologic changes observed in patients. Previously, we identified the estrogen-related receptor gamma (ERRγ) agonist T112 as an hiPSC-CM maturation inducer using a 2D assay (Miki et al., 2021). While T112 enables the maturation of hiPSC-CMs acutely (approximately 8 days of treatment), whether ERRγ activation enhances the organization and maturation of ECTs for disease modeling of HCM remains unclear.

This study aimed to establish a method for generating mature ECTs and isogenic HCM models with malignant and nonmalignant pathogenic sarcomere gene mutations using T112. As we had anticipated, T112-treated ECTs showed mature phenotypes. Moreover, combining T112 and mechanical stretching further enhanced morphological and metabolic maturation. Using isogenic hiPSCs with malignant pathogenic sarcomere mutations (MYH7 R719Q) and those with nonmalignant pathogenic sarcomere mutations (MYBPC3 G115*), we demonstrated that this combinatorial approach allows for the manifestation of clinically relevant phenotypes, including cardiomyocyte hypertrophy and non-cardiomyocyte dysfunctions such as fibronectin accumulation. On the other hand, consistent with the malignancy associated with the two pathogenic mutations we examined in this study, we revealed that there are phenotypic differences between HCM ECTs with MYH7 R719Q and MYBPC3 G115* mutations. Altogether, the combination of T112 and mechanical stretching enhanced the maturation of ECTs over a short duration and led to a manifested HCM model, wherein we could observe evident differences in disease phenotypes between malignant and nonmalignant pathogenic sarcomere mutations.

RESULTS

T112 enhances TNNI3 expression and sarcomere maturation in ECTs

The sarcomeric TNNI gene switches from the fetal isoform, TNNI1, to the adult isoform, TNNI3, during development (Bhavsar, 1991). We previously discovered the ERRγ agonist T112 to promote hiPSC-CM maturation using the dual reporter hiPSC line integrating emerald green fluorescent protein (EmGFP) and mCherry genes into the TNNI1and TNNI3 loci, respectively (Miki et al., 2021). To confirm whether T112 promotes ECT maturation, we generated strip-like ECTs with both sides anchored, using a mixture of 10% normal human dermal fibroblasts (NHDFs) and 90% non-purified hiPSC-CMs derived from the dual reporter hiPSCs. In CMs derived from these dual reporter induced pluripotent stem cells (iPSCs), approximately 80% of the cells were EmGFP-positive cardiomyocytes (Figure S1A). From day 7 after fabrication, we cultured ECTs in the presence of T112 for an additional 8 days. Flow cytometric and imaging analyses showed that T112 treatment increased the expression of mCherry (TNNI3) in cardiomyocytes as compared to vehicle (DMSO) treatment (Figures S1B–S1D). There were no differences in the expression of mCherry between 3 μM, the optimal concentration in embryoid body (EB) culture, and 10 μM (Figures S1B–S1D). Moreover, ECTs treated with either 3 or 10 μM T112 had clearer z-disc-aligned sarcomeres compared to control ECTs (Figure S1E). We thus used 3 μM T112 for all subsequent experiments.

Combined T112 treatment and mechanical stretching enhance ECT maturation

Mechanical stretching was shown previously to enhance the maturation of ECTs composed of cardiomyocytes and cardiovascular progenitor cells derived from pluripotent stem cells (Leonard et al., 2018; Ruan et al., 2016). Therefore, we investigated whether combined T112 treatment and mechanical stretching could further promote ECT maturation. The Flexcell system can mechanically stretch ECTs by vacuum suction under the culture plate, allowing maximal elongation of up to 10% (Figure 1A). ECTs were cultured using 10% elongation stimulation at 1 Hz in the

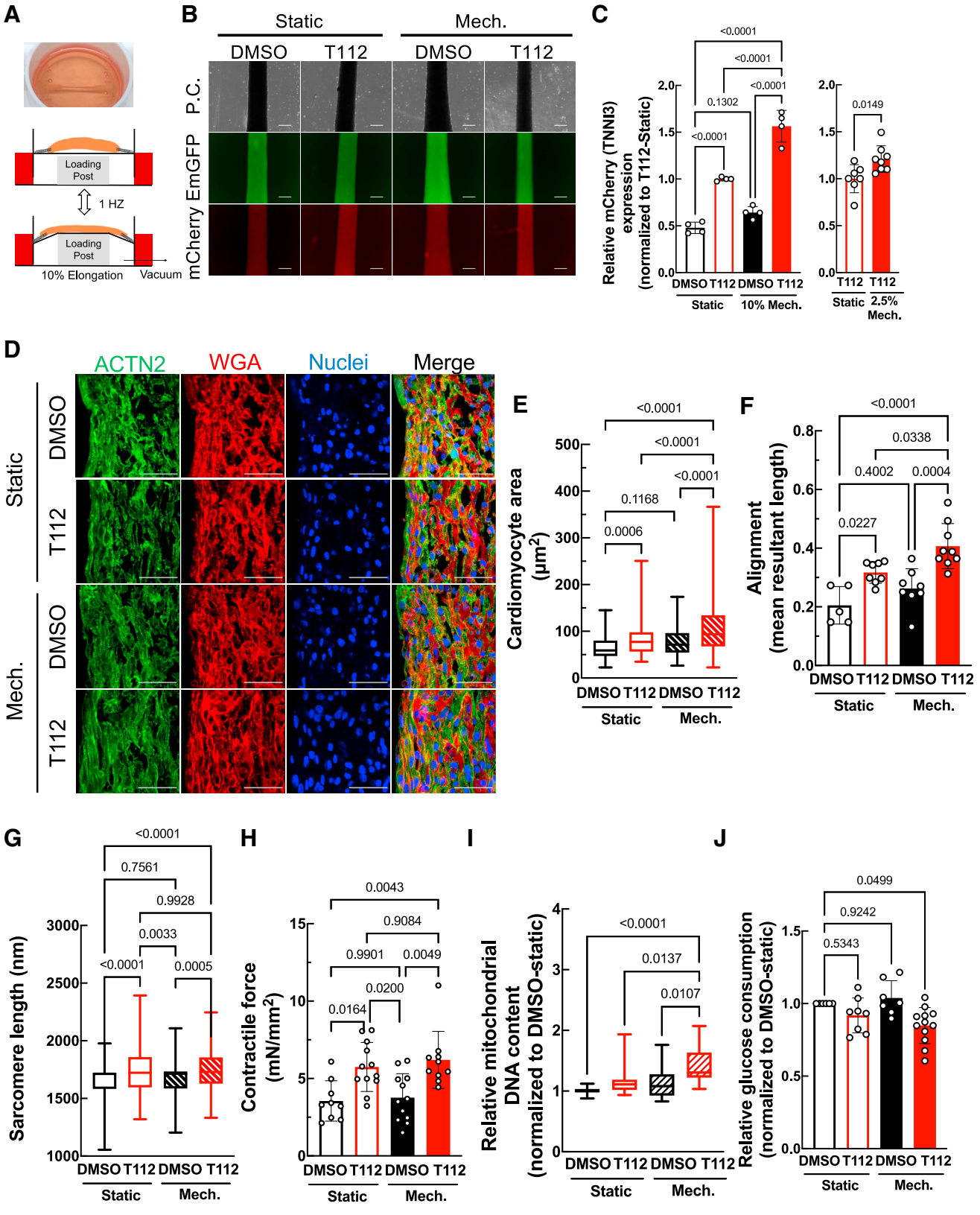

(legend on next page)

presence of T112 for 8 days. mCherry expression in the T112-treated ECTs with mechanical stretching (T112-mech) was significantly higher (1.6-fold increase) than that in the T112-treated static ECT cultures (T112-static) (Figures 1B, 1C, and S2A). ECTs treated with T112 and subjected to 2.5% elongation (the minimum setting) showed a mild increase of mCherry expression (1.2-fold increase) compared to T112-static (Figure 1C). These results indicate that this additive effect depends on the amount of stretching ECTs experienced in conjunction with T112 treatment. Both control and T112-treated ECTs subjected to mechanical stretching (DMSO-mech and T112-mech, respectively) showed increased EmGFP expression compared to static ECT cultures treated with DMSO (DMSO-static) (Figure S2B), even though TNNI1 expression was comparable among these ECTs (Figure S3A).

We further assessed the cardiac maturation of each ECT treatment group by measuring cardiomyocyte size. Notably, we observed a significant increase in cardiomyocyte size by T112 treatment (T112-static vs. DMSO-static), further enhanced in the T112-mech group (Figures 1D and 1E). Sarcomere alignment was affected similarly, with the T112-mech group displaying the highest anisotropy (Figure 1F). The sarcomere length of T112-static ECTs was significantly longer than that of DMSO-static and DMSO-mech ECTs, and mechanical stretching failed to increase sarcomere length further for the T112-mech group (Figure 1G). As with sarcomere length, the contractile force was significantly higher in T112-mech ECTs (Figure 1H). Next, we examined the effect on metabolic maturation. Mitochondrial content increased for ECTs with combinatorial treatment (T112-mech) (Figure 1I). Moreover, glucose consumption was decreased only in T112-mech compared to DMSO-static (Figure 1J). These data indicate that combined T112 treatment and mechanical stretching enhanced both the structural and metabolic maturation of ECTs. Notably, while T112 treatment improved several parameters, mechanical stretching alone had no effects.

Next, we compared the gene expression profiles of ECTs from each treatment group by RNA sequencing (RNA-seq). Principal-component analysis (PCA) showed that the DMSO-treated (DMSO-static and DMSO-mech) and T112-treated (T112-static and T112-mech) conditions were separated, indicating the impact of T112 treatment on global gene expression (Figure 2A). We first performed Gene Ontology (GO) enrichment analysis by focusing on "cellular components" of the differentially expressed genes (DEGs) (Data S1) and found that all stimulation conditions upregulated gene sets related to myofibril, sarcomere, and contraction fiber (Figure 2B). Furthermore, T112 treatment with or without mechanical stimulation (T112-static and T112-mech) also enhanced the expression of genes related to I-band and z-discs (Figure 2B). In addition, GO enrichment analysis of the DEGs for "biological process" revealed that T112 decreased the cell cycle of ECTs (Figure S3B; Data S2). These results indicate that T112 treatment induces global gene expression patterns toward ECT maturation.

Next, we examined the expression patterns of individual genes related to cardiac maturation. Although the expression of ion-channel-related genes did not change with maturation, the expression of SR/calcium handling and sarcomere-related genes, such as *CAMK2B*, *MYH7*, *TNNI3*,

Figure 1. Functional characterization of mature ECTs

(A) Representative tissue image and schematic of mechanical stretching.

(B) Phase contrast (upper), EmGFP fluorescence (TNNI1, middle), and mCherry fluorescence (TNNI3, lower) images of day-15 ECTs treated with DMSO or 3 μM T112, in static condition or with mechanical stretching (10% elongation at 1 Hz) (DMSO-static, T112-static, DMSO-mech, and T112-mech). Scale bar, 500 μm. See also Figures S1A and S1B.

(C) Quantification of mCherry expression of day-15 ECTs with DMSO or 3 μM T112, in static condition or with mechanical stretching (2.5% or 10% elongation at 1 Hz) from three independent experiments (n = 4–8). See also Figures S1C, S1D, S2A, and S2B.

(D) Representative immunostaining images of day-15 DMSO-static, T112-static, DMSO-mech, or T112-mech ECTs for wheat germ agglutinin (WGA) (red), ACTN2 (green), and DNA (blue). Scale bar, 50 μm. See also Figure S1E.

(E) Quantification of cardiomyocyte area of day-15 DMSO-static, T112-static, DMSO-mech, and T112-mech ECTs from three independent experiments (n = 110–164).

(F) Quantification of sarcomere alignment of day-15 DMSO-static, T112-static, DMSO-mech, and T112-mech ECTs from five independent experiments (n = 5–9).

(G) Quantification of sarcomere length of day-15 DMSO-static, T112-static, DMSO-mech, or T112-mech ECTs from three independent experiments (n = 90–120).

(H) Quantification of contractile force in DMSO-static, T112-static, DMSO-mech, or T112-mech ECTs from four independent experiments (n = 9–12).

(I) Quantification of mitochondrial DNA content of day-15 DMSO-static, T112-static, DMSO-mech, or T112-mech ECTs from nine independent experiments (n = 15–18). Data are shown relative to the DMSO-static group in each experimental batch.

(J) Quantification of glucose consumption of DMSO-static, T112-static, DMSO-mech, or T112-mech ECTs from six independent experiments (n = 6–12). Data presented as the mean ± SD (C, F, H, and J) or in a boxplot (E, G, and I). All statistical analyses were performed using two-way ANOVA with Tukey's multiple comparison test.

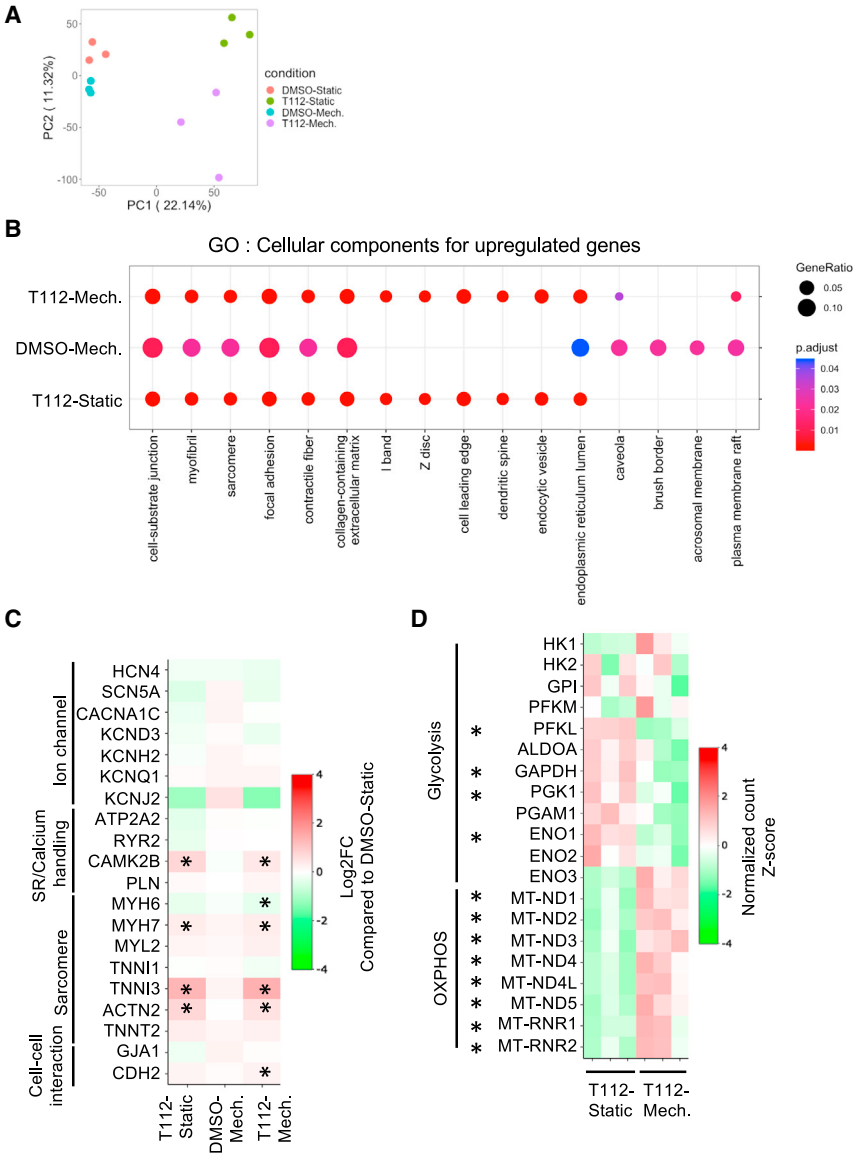

Figure 2. RNA-seq analysis of ECTs

(A) PCA of RNA-seq of day-15 DMSO-static, T112-static, DMSO-mech, or T112-mech ECTs from three independent experiments (n = 3).

(B) Gene Ontology (GO) cell component terms enriched in upregulated differentially expressed genes (DEGs) compared with DMSO-static (log2 FC > 0, q < 0.05). The color indicates the p value. Circle size indicates the ratio of the number of genes containing each GO term to the number of DEGs. See also Figures S3A and S3B and Data S1 and S2.

(C) Heatmap showing the expression of selected genes. The color bar indicates log2 FC compared to the DMSO-static group. Asterisk (*) indicates significant expression compared to the DMSO-static group (q value <0.05).

(D) Heatmap showing expression of selected genes. The color bar indicates the *Z* score of the normalized count. Asterisk (*) indicates significant expression compared to the T112-static group (q value <0.05). See also Figure S6D.

and *ACTN2*, was significantly increased in T112-static and T112-mech ECTs compared to that in DMSO-static ECTs (Figure 2C). Notably, while mechanical stimulation of T112-treated ECTs significantly reduced *MYH6* expression, which decreases during maturation *in vivo*, the expression of *CDH2*, known as a component of the adherens junction of cardiomyocytes, increased. These differences were not observed in T112-static ECTs (Figure 2C), thus illustrating the importance of combining chemical and mechanical stimulation.

We compared the gene expression profiles between T112-static and T112-mech ECTs to examine further the differences induced by mechanical stimulation of ECTs during T112 treatment. In T112-mech ECTs, oxidative phosphorylation (OXPHOS)-related genes, such as *MT-ND1*, *MT-ND2*, *MT-ND3*, *MT-ND4*, *MT-ND4L*, *MT-ND5*, *MT-RNR1*, and *MT-RNR2*, were significantly upregulated compared to T112-static ECTs (Figure 2D). In contrast, the expression of glycolysis-related genes, such as *ENO1*, *GAPDH*, *PFKL*, and *PGK1*, was significantly decreased in T112-mech ECTs compared to that in T112-static ECTs (Figure 2D). These results suggest that mechanical stretching together with T112 treatment enhances the metabolic shift from glycolysis to oxidative phosphorylation as ECTs mature.

In summary, mechanical stretching alone did not result in functional maturation of ECTs, as shown in Figure 1, but the gene expression pattern trended toward improved

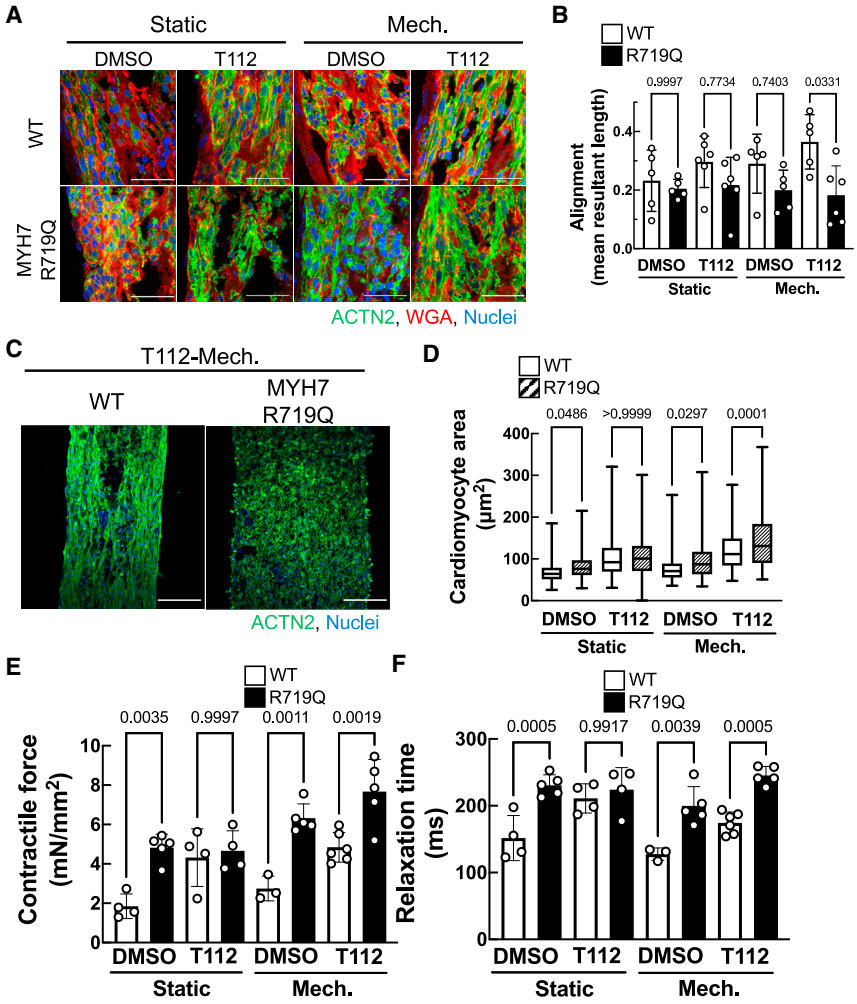

Figure 3. Phenotype characterization of MYH7 R719Q ECTs

(A) Representative immunofluorescence images of day-15 WT or MYH7 R719Q ECTs with DMSO-static, T112-static, DMSO-mech, or T112-mech treatment for WGA (red), ACTN2 (green), and DNA (blue). Scale bar, 50 μm. See also Figures S4A–S4D.

(B) Quantification of sarcomere alignment of day-15 WT or MYH7 R719Q ECTs with DMSO-static, T112-static, DMSO-mech, or T112-mech treatment from five independent experiments (n = 5–6).

(C) Representative immunofluorescence images of day-15 WT or MYH7 R719Q ECTs with T112-mech treatment for ACTN2 (green) and DNA (blue). Scale bar, 200 μm.

(D) Quantification of cardiomyocyte area of day-15 WT or MYH7 R719Q ECTs with DMSO-static, T112-static, DMSO-mech, or T112-mech treatment from four independent experiments (n = 100–154).

(E and F) Quantification of contractile force (E) and 90% relaxation time (F) in WT or MYH7 R719Q ECTs with DMSO-static, T112-static, DMSO-mech, or T112-mech treatment from three to five independent experiments (n = 3–6). See also Figure S4E. Data are presented as the mean ± SD (B, E, and F) or in a boxplot (D). All statistical analyses were performed using two-way ANOVA with Tukey's multiple comparison test.

maturation. The combination of mechanical stretching and T112 treatment enhanced the expression of sarcomere-related genes and shifted the energy supply from glycolysis to oxidation phosphorylation in ECTs.

Combinatorial treatment enhances the diversity of HCM phenotypes observed in MYH7 R719Q ECTs

To confirm whether our new combinatorial treatment could model HCM with a malignant pathogenic sarcomere gene mutation in ECTs, we used the CRISPR-Cas9 system to generate an isogenic hiPSC line harboring a heterozygous MYH7 R719Q mutation (Figure S4A), a malignant pathogenic sarcomere gene mutation in HCM patients (Van Driest et al., 2002). The genome-edited MYH7 R719Q iPSCs showed a normal karyotype (Figure S4B) and did not display any defects in differentiation efficiency (Figure S4C). Wild-type (WT) and R719Q mRNAs were equally expressed in hiPSC-CMs with the MYH7 R719Q mutation (Figure S4D).

We first tested whether our MYH7 R719Q ECTs could recapitulate the structural abnormalities, such as myofibril disarray and cardiomyocyte hypertrophy, presented in HCM. Myofibril alignment improved with enhanced maturation in WT ECTs but not for all conditions examined in MYH7 R719Q ECTs (Figures 3A–3C). The difference in myofibril alignment between WT and MYH7 R719Q ECTs was observed only in the T112-mech treatment group (Figures 3A–3C). On the other hand, cardiomyocyte size was significantly larger in MYH7 R719Q than in WT DMSO-static, DMSO-mech, and T112-mech ECTs (Figures 3A and 3D). Notably, the differences in cardiomyocyte size were more significant in MYH7 R719Q ECTs treated by our combinatorial maturation method (DMSO-static, $p = 0.0486$; DMSO-mech, $p = 0.0297$; T112-mech, $p = 0.0001$) (Figure 3D). MYH7 R719Q ECTs showed higher contractile force (Figure 3E) and longer relaxation time (Figure 3F) than WT ECTs in DMSO-static, DMSO-mech, or T112-mech treatment groups, suggesting that the

MYH7 R719Q mutation caused diastolic dysfunction. In contrast, contraction times were comparable under all conditions (Figure S4E). Altogether, we successfully recapitulated in our mature ECTs several characteristic HCM phenotypes, including myofibril disarray, hypertrophy, hypercontractility, and diastolic dysfunction, for the malignant HCM sarcomere mutation, MHY7 R719Q. In contrast, immature ECTs displayed only hypertrophy, hypercontractility, and diastolic dysfunction, indicating that the combinatorial treatment provides better *in vitro* modeling of HCM phenotypes.

T112 treatment and mechanical stretching together manifest the hypertrophy phenotype of ECTs with a MYBPC3 truncation mutation

The sudden cardiac death (SCD) risk of pediatric HCM with pathogenic sarcomere gene mutations such as MYH7 R719Q is higher than adult-onset HCM (Miron et al., 2020). As expected, ECTs robustly manifested the HCM phenotypes caused by the MYH7 R719Q mutation. We thus assessed whether this combinatorial method is also helpful for modeling nonmalignant HCM pathogenic sarcomere gene mutations. Among HCM patients, MYBPC3 truncation mutations are one of the most frequent mutations, and the clinical courses are similar regardless of mutation location since the loss of function is thought to cause HCM (Helms et al., 2020; Marston et al., 2009). HCM with MYBPC3 truncation mutations is known as adult-onset HCM, diagnosed at an average age of approximately 39 years (Helms et al., 2020), and is thus defined as a set of nonmalignant pathogenic mutations. However, no report to date has produced an accurate *in vitro* isogenic HCM model using ECTs with MYBPC3 mutations that present a hypertrophic phenotype. Therefore, we generated an hiPSC line with a heterozygous MYBPC3 truncation mutation (MYBPC3 G115*) using CRISPR-Cas9 (Figure S5A).

We confirmed the sequences of both WT MYBPC3 and the inserted fragment containing the MYBPC3 G115* mutation in hiPSCs (Figure S5B). The generated hiPSCs had a normal karyotype (Figure S5C), and genome editing did not affect differentiation efficiency (Figure S4C). In hiPSC-CMs with the mutation, MYBPC3 mRNA and protein expressions were reduced to approximately 50% of WT levels (Figures 4A, 4B, and S5D). Next, we measured cardiomyocyte size and myofibril alignment of ECTs. Although there was no difference in cardiomyocyte size between WT and MYBPC3 G115* ECTs under conventional culture conditions (Figure S5E), our combinatorial method manifested a hypertrophic phenotype in this HCM model (Figures 4C and 4D). On the other hand, unlike ECTs with the MYH7 R719Q mutation, MYBPC3 G115* ECTs did not show any significant myofibril disarray compared to WT ECTs (Figure 4E). For contractile properties, although the contractile force and time were comparable (Figures 4F and S5F), we observed prolonged relaxation time in ECTs with the MYBPC3 G115* mutation in contrast to WT ECTs (Figure 4G). Collectively, in ECTs with a clinically nonmalignant pathogenic sarcomere gene mutation (i.e., MYBPC3 G115*), our combinatorial method enabled the manifestation of HCM phenotypes, such as hypertrophy and diastolic dysfunction.

ECTs with MYH7 R719Q and MYBPC3 G115* mutations have transcriptional characteristics of HCM

Next, we performed transcriptome analysis of WT ECTs and ECTs with MYH7 R719Q or MYBPC3 G115* mutations. PCA showed that the transcriptome profiles were predominantly separated by PC1 (Figure 5A). To characterize these HCM models, we examined the DEGs by GO enrichment analysis (Data S3). Both mutations upregulated gene sets related to contraction, such as muscle system process, muscle contraction, striated muscle contraction, and striated muscle tissue development (Figure 5B). Additionally, the gene sets specifically upregulated in MYH7 R719Q ECTs were related to the extracellular matrix (ECM), such as ECM organization, extracellular structure organization, and external encapsulating structure organization (Figure 5B). These results are consistent with the proteomics data of patients with HCM, which showed high expression of proteins related to fibrosis and contraction (Schuldt et al., 2021), indicating that these HCM models could faithfully mimic the changes in HCM hearts.

Moreover, we performed Disease Ontology (DO) semantic and enrichment analysis (Yu et al., 2015). Myopathy-related DO terms, such as myopathy, muscle tissue disease, and muscular disease, were at the top of the enriched DO term list in both ECTs with MYH7 R719Q and MYBPC3 G115* mutations (Table 1). In addition, the DO term of hypertrophic cardiomyopathy was significantly enriched in both MYH7 R719Q and MYBP3 G115* ECTs (DOID:11984, MYH7 R719Q, p = 0.0035 and MYBPC3 G115*, p = 8.34E−09) (Data S4). The data from these enrichment analyses support that ECTs with MYH7 R719Q or MYBPC3 G115* mutations transcriptionally recapitulated broad aspects of HCM phenotypes.

We confirmed the expression pattern of representative genes known to change in HCM patients. In MYH7 R719Q ECTs, the expression of sarcomere and fibrosis genes, such as *MYH7*, *TNNI3*, *MYL2*, *TGFB1*, *COL1A2*, *COL4A1*, *COL4A2*, *COL6A1*, *COL6A2*, *COL6A3*, *COL7A1*, and *COL15A1*, were significantly upregulated (Figure 5C, upper panel). In ECTs with the MYBPC3 G115* mutation, sarcomere genes, such as *MYH7*, *TNNI3*, and *NPPB*, were significantly upregulated (Figure 5C, upper panel).

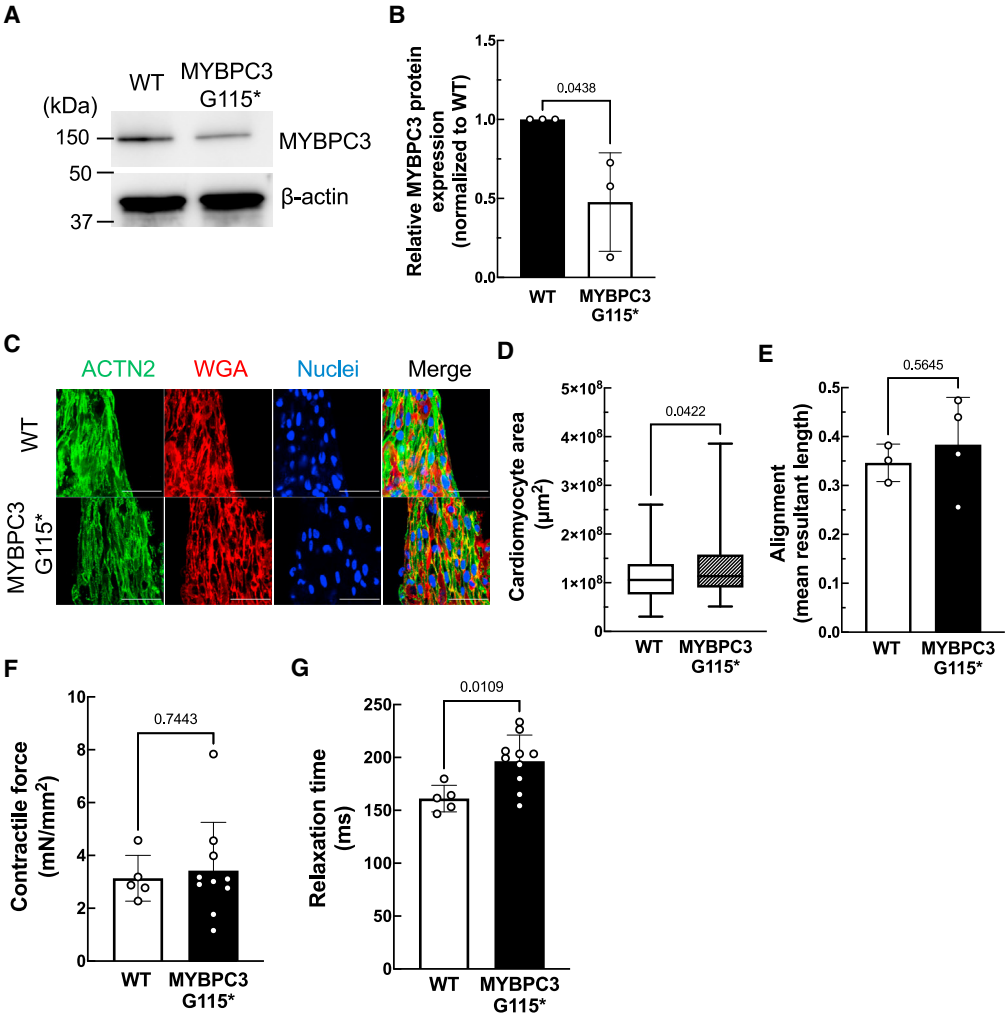

Figure 4. Phenotype characterization of MYBPC3 G115* ECTs

(A) Representative western blotting images of day-29 WT or MYBPC3 G115* EB lysate using anti-MYBPC3 (upper) and anti-β-actin antibodies (lower). The molecular-weight ladder is shown on the left side. See also Figures S4D and S5A–S5D.

(B) Quantification of MYBPC3 expression normalized by β-actin expression from three independent experiments (n = 3).

(C) Representative immunofluorescence images of day-15 WT or MYBPC3 G115* ECTs with T112-mech treatment for WGA (red), ACTN2 (green), and DNA (blue). Scale bar, 50 μm.

(D) Quantification of cardiomyocyte area of day-15 WT and MYBPC3 G115* ECTs with T112-mech treatment from three independent experiments (n = 70–88). See also Figure S5F.

(E) Quantification of sarcomere alignment on day-15 WT and MYBPC3 G115* ECTs with T112-mech treatment from three independent experiments (n = 3–4).

(F and G) Quantification of contractile force (F) and 90% relaxation time (G) in WT or MYBPC3 G115* ECTs with T112-mech treatment from four independent experiments (n = 5–10). See also Figure S5E. Data are presented as the mean ± SD (B and E–G) or in a boxplot (D). All statistical analyses were performed using unpaired t tests.

Additionally, *MYBPC3* expression was significantly downregulated in ECTs with the MYBPC3 G115* mutation (Figure 5C, upper panel).

In MYH7 R719Q ECTs, glycolysis-related genes, such as *HK1*, *ENO2*, and *PKM*, were upregulated (Figure 5C, lower panel), with the GO term nucleotide metabolic process (GO: 0009117, p = 0.0025), related to glycolysis, enriched in upregulated genes in ECTs with the MYH7 R719Q mutation (Data S3). Indeed, MYH7 R719Q ECTs consumed more glucose in the culture medium than WT or MYBPC3 G115* ECTs (Figure 5D), indicating activated glycolysis in the MYH7 R719Q ECTs. Additionally, we checked these changes in the ECM in each model. Although the increased mRNA expression of fibronectin (*FN1*), also known as

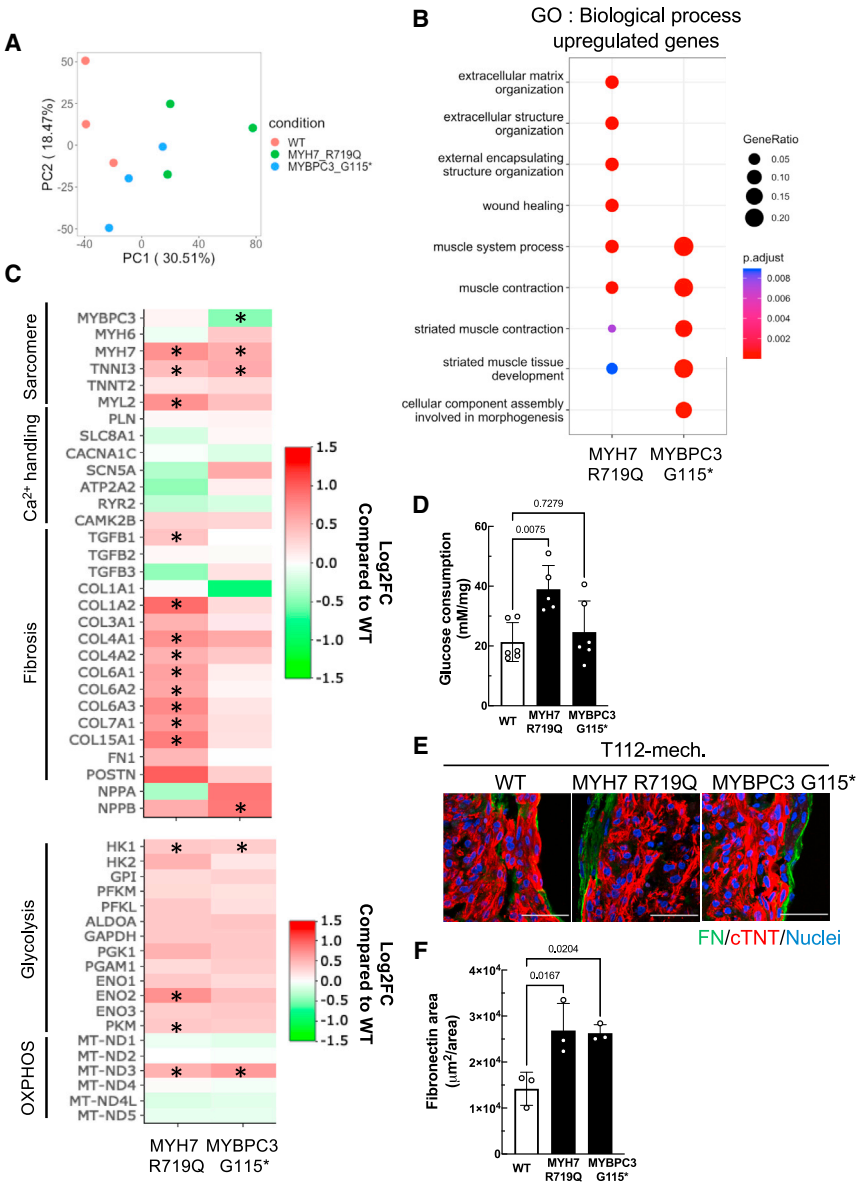

Figure 5. RNA-seq analysis of HCM model using isogenic iPSCs

(A) PCA of RNA-seq data of day-15 WT, MYH7 R719Q, or MYBPC3 G115* ECTs with T112-mech treatment from three independent experiments (n = 3).

(B) GO biological process terms enriched in upregulated DEGs compared to WT (log2 FC > 0, q < 0.05). The color indicates the p value. Circle size indicates the ratio of the number of genes containing each GO term to the number of DEGs. See also Data S3.

(C) Heatmap showing the expression of selected genes. The color bar indicates log2 FC compared to WT. Asterisk (*) indicates significant expression change compared to WT (q value <0.05).

(D) Quantification of glucose consumption of WT, MYH7 R719Q, or MYBPC3 G115* ECTs cultured for 4 days under static conditions after T112 treatment and mechanical stimulation from three independent experiments (n = 5–6).

(E) Representative immunostaining images of day-15 WT, MYH7 R719Q, or MYBPC3 G115* ECTs with T112-mech treatment for fibronectin (green), cardiac troponin T (red), and DNA (blue). Scale bar, 50 μm.

(F) Quantification of fibronectin-positive area of day-15 WT, MYH7 R719Q, or MYBPC3 G115* ECTs with T112-mech treatment from three independent experiments (n = 3). See also Figure S5G. Data are presented as the mean ± SD (D and F). Statistical analyses were performed using one-way ANOVA with Dunnett's multiple comparison test (D and F).

cardiac fibrosis factor, was insignificant, fibronectin protein accumulation was confirmed in the non-cardiomyocytes of ECTs with MYH7 R719Q or MYBPC3 G115* mutations compared to WT ECTs (Figures 5E and 5F). In contrast, there was no difference in fibronectin protein accumulation under conventional culture conditions (Figure S5G). Therefore, these results indicate that ECTs treated with T112 and mechanical stretching can also recapitulate functional changes in non-cardiomyocytes, such as fibroblasts.

Altogether, these results indicate that our method, based on ERRγ activation and mechanical stretching, facilitates the maturation of ECTs. This approach allows for the generation of HCM models that harbor malignant or nonmalignant pathogenic sarcomere gene mutations and represents a high-resolution method to distinguish disease severity caused by distinct pathogenic mutations, thus modeling more faithfully the heart tissues of different HCM patients.

T112 treatment and mechanical stretching robustly enhance ECT maturity and manifest HCM phenotypes

We confirmed the robustness of this maturation method using another hiPSC line, 1390C1. T112-mech ECTs exhibited increased cardiomyocyte size and sarcomere length and alignment (Figures 6A–6D). Additionally, T112-mech

Table 1. DO semantic and enrichment analysis

	ID	Description	p value
MYH7 R719Q	DOID:423	myopathy	2.99E−08
	DOID:66	muscle tissue disease	2.99E−08
	DOID:0080000	muscular disease	6.04E−08
	DOID:0060100	musculoskeletal system cancer	4.50E−07
	DOID:10155	intestinal cancer	5.08E−07
MYBPC3 G115*	DOID:0060036	intrinsic cardiomyopathy	8.97E−10
	DOID:423	myopathy	8.98E−10
	DOID:66	muscle tissue disease	8.98E−10
	DOID:0080000	muscular disease	1.17E−09
	DOID:0050700	cardiomyopathy	1.98E−09

Table of the top five DO terms for upregulated DEGs in MYH7 R719Q and MYBPC3 G115* ECTs (see also Data S4).

treatment significantly enhanced the contractile force (Figure 6E). Next, we examined whether this independent hiPSC line could reproduce the HCM phenotypes observed in MYH7 R719Q and MYBPC3 G115* ECTs derived from 1390D4 when subjected to our new maturation method. Similar to the 1390D4 observations, although 1390C1 iPSC-CMs with the MYH7 R719Q mutation expressed both MYH7 WT and R719Q mRNA (Figure S6A), MYBPC3 G115* iPSC-CMs derived from 1390C1 hiPSCs showed a decrease in MYBPC3 expression (Figure S6B). Genome editing also did not affect the differentiation efficiency (Figure S6C). Sarcomere disarray was observed in 1390C1-derived MYH7 R719Q ECTs subjected to T112-mech treatment (Figure 6F). Cardiomyocyte hypertrophy was evident in the MYBPC3 G115* ECTs derived from 1390C1 hiPSCs when subjected to T112-mech treatment (Figure 6G). Furthermore, fibronectin accumulation in the non-cardiomyocyte area was observed in MYBPC3 G115* ECTs with T112-mech treatment (Figures 6H and 6I). These results demonstrate that ECT maturation using this method robustly manifests HCM phenotypes reproducibly.

DISCUSSION

In this study, we established a method for generating mature ECTs and HCM models derived from isogenic hiPSCs in a shorter time using an ERRγ agonist, T112, that accelerates iPSC-CM maturation.

Establishing an accelerated method for maturing ECTs is crucial for cost-effective drug development. Several protocols require 2–5 weeks to produce mature ECTs (Leonard et al., 2018; Ronaldson-Bouchard et al., 2018; Ruan et al., 2016). In this study, we successfully promoted ECT maturity to manifest HCM phenotypes after only 8 days by combining chemical and mechanical stimulation.

Although it was previously shown that 2 weeks of mechanical stretching promotes ECT maturation (Leonard et al., 2018; Ruan et al., 2016), ECTs treated with mechanical stretching alone (DMSO-mech) did not show any significant enhancement in functional maturity compared to control (DMSO-static) ECTs (Figure 1). In contrast, mechanical stretching in the presence of T112 induced several functional changes, including cardiomyocyte size, sarcomere alignment, and mitochondrial content (Figures 1E, 1F, and 1I). Therefore, these results suggest that other maturation methods, such as electrophysiological stimulation, high fatty acid culture conditions (Funakoshi et al., 2021), and hormone stimulation (Seeger et al., 2019), in combination with T112 treatment and mechanical stretching may further expedite ECT maturation within an even shorter period.

Regarding the maturity of ECTs treated using this method, it was reported that glucose uptake is diminished during the late gestational and early postnatal stages to adapt to the transition from glycolysis to high-energy-production pathways before increasing fatty acid oxidation (Piquereau and Ventura-Clapier, 2018). Due to technical challenges associated with metabolic analysis of ECTs, we did not undertake an in-depth analysis of metabolic profiles of our ECTs. However, considering the results of our study, which demonstrate reduced glucose consumption, increased mitochondrial DNAs, and a gene expression shift from glycolysis to OXPHOS, along with sustained TNNI1 expression (Figures 1I, 1J, 2D, and S3A), it is reasonable to suggest that ECTs subjected to the combinatorial treatment more closely resemble neonatal hearts in terms of maturity.

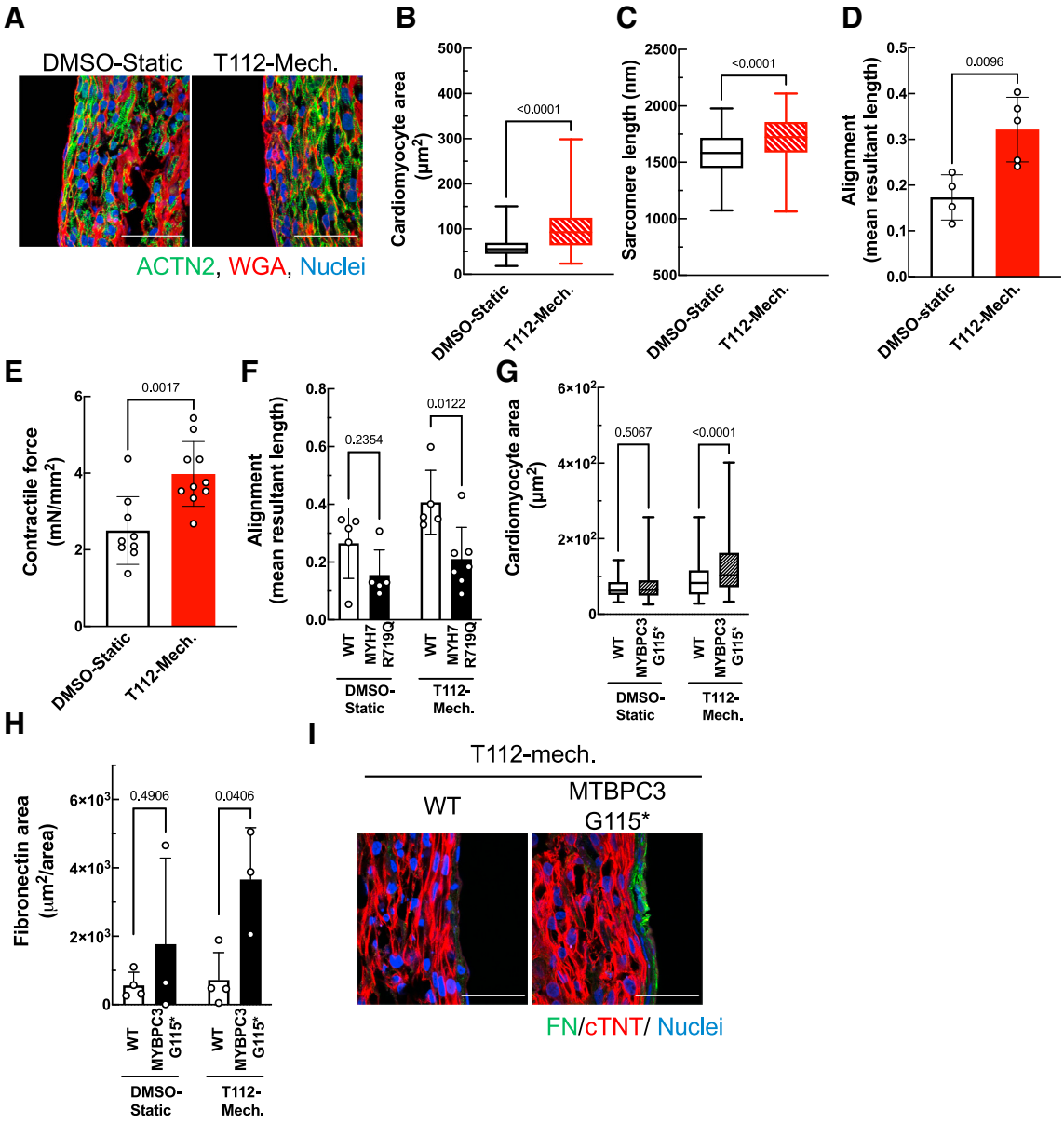

Figure 6. Robustness of T112 treatment and mechanical stretching

(A) Representative immunostaining images of day-15 ECTs with DMSO-static or T112-mech treatment for WGA (red), ACTN2 (green), and DNA (blue). Scale bar, 50 μm.

(B) Quantification of cardiomyocyte area of day-15 DMSO-static or T112-mech ECTs from three independent experiments (n = 105–287).

(C) Quantification of sarcomere length of day-15 of ECTs with DMSO-static or T112-mech treatment from three independent experiments (n = 72).

(D) Quantification of sarcomere alignment of day-15 DMSO-static or T112-mech ECTs from three independent experiments (n = 4–5).

(E) Quantification of contractile force in DMSO-static or T112-mech ECTs from four independent experiments (n = 9–10).

(F) Quantification of sarcomere alignment of day-15 WT or MYH7 R719Q ECTs with DMSO-static or T112-mech treatment from four independent experiments (n = 5–7). See also Figures S6A and S6C.

(G) Quantification of cardiomyocyte area of day-15 WT or MYBPC3 G115* ECTs with DMSO-static or T112-mech treatment from three to four independent experiments (n = 95–159). See also Figures S6B and S6C.

(H) Quantification of fibronectin-positive area of day-15 WT or MYBPC3 G115* ECTs with DMSO-static or T112-mech treatment from three independent experiments (n = 3–4).

(legend continued on next page)

Using our new modified culture conditions, we successfully reproduced several HCM phenotypes using ECT models, including hypertrophy, hypercontractility, and diastolic dysfunction in ECTs with the MYH7 R719Q mutation. In contrast, myofibril disarray and fibronectin accumulation emerged only under our newly defined maturation conditions, T112-mech. Our results indicate that HCM progression may require functional maturation, suggesting this platform enables the detailed studies of HCM pathogenic mechanisms and the efficacy evaluation of therapeutic agents at various stages of HCM progression.

Additionally, we observed hypertrophic changes only under defined maturation conditions in ECTs with the MYBPC3 G115* mutation. Under conventional conditions (static condition culture without T112), no apparent hypertrophy was observed in MYBPC3 G115* ECTs. Moreover, we did not only detect functional and structural changes in cardiomyocytes but also found ECM accumulation by non-cardiomyocytes in ECTs possessing either of the mutations examined. These results yielded two critical insights: (1) ECT maturation is essential to the *in vitro* progression of HCM phenotypes, and (2) the severity of *in vitro* HCM models is correlated with the malignancy of the pathogenic sarcomere mutations.

It was reported using monolayer assays that Danon disease patient hiPSC-derived CMs failed to show hypertrophy compared to healthy subjects in the absence of an accelerated maturation process; however, these hiPSC-CMs displayed hypertrophy when they were treated with galactose, oleic acid, and palmitic acid to enhance maturation (Knight et al., 2021). In this study, although T112 treatment alone eliminated the observed HCM phenotypes, such as hypertrophy (Figure 3D), hypercontractility (Figure 3E), and diastolic dysfunction (Figure 3F), in MYH7 R719Q ECTs when compared to control (DMSO), treatment with T112 under mechanical stretching (T112-mech) showed additional HCM phenotypes, including myofibril disarray and fibronectin accumulation, indicating that mechanical-stretching-based maturation is crucial for the full manifestation of HCM phenotypes. These results also suggest a possible relationship between ERRγ signaling and HCM progression. Further studies are required to elucidate the potential role of ERRγ in the pathogenesis of HCM.

Malignancy of pathogenic sarcomere mutations appears to be associated with more severe defects in our *in vitro* HCM models. Mature ECTs with the malignant pathogenic sarcomere mutations, MYH7 R719Q, showed a variety of abnormal phenotypes, such as myofibril misalignment, hypertrophy, hypercontraction, diastolic dysfunction, upregulated glycolysis, and fibrotic change. In contrast, mature ECTs with nonmalignant pathogenic sarcomere mutations, MYBPC3 G115*, showed a subset of these aberrant phenotypes (i.e., hypertrophy, diastolic dysfunction, and fibronectin accumulation). Although a systemic analysis of additional mutations will be necessary, our findings suggest that this accelerated CM maturation model may help predict malignant pathogenic sarcomere mutations for risk stratification.

Regarding the distinct contractile dysfunctions observed in HCM with pathogenic sarcomere gene mutations, although diastolic dysfunction is a common clinical feature of HCM, whether hypercontractility is a phenotype commonly caused by sarcomere gene mutations remains controversial (Mosqueira et al., 2019). In this study, MYH7 R719Q ECTs showed hypercontraction and diastolic dysfunction, whereas MYBPC3 G115* ECTs displayed only diastolic dysfunction. In previous reports, ECTs with the MYBPC3 W792Vfs*41 mutation generated higher twitch force than isogenic WT ECTs (Cohn et al., 2019), and hiPSC-CMs with the MYBPC3 R943* homozygous mutation treated with Dex/T3/IGF showed a decrease in contraction velocity in a monolayer assay (Seeger et al., 2019). Furthermore, it has been documented that *in vitro* motility assays using tissue explants derived from HCM hearts did not necessarily represent hypercontraction (Mosqueira et al., 2019). Therefore, along with our findings presented here, hypercontractility in HCM may largely depend upon the type of sarcomere mutation involved.

In earlier studies, cardiomyocytes of HCM patients showed decreased *ATP2A2* expression and exhibited abnormal calcium handling (Somura et al., 2001). However, our ECT model did not reveal any significant change in *ATP2A2* expression in ECTs with either MYH7 R719Q or MYBPC3 G115* mutations compared to WT ECTs (Figure 5C). Although adult cardiomyocytes have higher expression of *SCN5A*, *KCNJ2*, *RYR2*, *ATP2A2*, and *CACNA1C* and lower expression of *HCN4* (Karbassi et al., 2020), T112-mech ECTs did not show any expression changes of these ion channel-related genes (Figure 2C), suggesting that there is likely room for further maturation in our HCM model to recapitulate the disease phenotype completely.

Hearts contain human cardiac fibroblasts (HCFs), not NHDFs. We thus conducted a comparison of ECT maturation by varying the mixture ratio (10%, 20%, and 30%)

(I) Representative immunostaining images of day-15 WT or MYBPC3 G115* ECTs with T112-mech treatment for fibronectin (green), cardiac troponin T (red), and DNA (blue). Scale bar, 50 μm. Data are presented in a boxplot (B, C, and G) or the mean ± SD (D–F and I). Statistical analyses were performed using unpaired t tests (B–E) or two-way ANOVA with Šídák's multiple comparison test (F and I) or Tukey's multiple comparison test (G).

of HCFs and NHDFs. While significant changes were observed in the expressions of *MYH6* and *RYR2*, no significant alterations were noted for *MYH7* or *TNNI3*, markers of sarcomere maturation. Furthermore, there were no significant changes detected in genes marking electrophysiological maturation, except for *RYR2* (Figure S6D). These results indicate that the percentage and types of non-cardiomyocytes exert only a minor influence on ECT maturation under our conditions. Nonetheless, further refinement of non-cardiomyocyte composition and proportions within ECTs might contribute to the development of cardiac tissues with a more adult-like phenotype.

In conclusion, we established a method to accelerate ECT maturation (8 days) by combining ERRγ activation and mechanical stretching. We also successfully generated an HCM model of ECTs with malignant and nonmalignant pathogenic sarcomere gene mutations (MYH7 R719Q and MYBPC3 G115*) using isogenic hiPSCs. Notably, while MYH7 R719Q ECTs displayed numerous HCM phenotypes, MYBPC3 G115* ECTs showed limited phenotypes. Therefore, not only does the accelerated maturation protocol, based on mechanical stretching and ERRγ activation, reduce the time required to produce mature ECTs but we have also demonstrated that they are applicable for modeling HCM, faithfully recapitulating the degree of malignancy caused by pathogenic sarcomere mutations.

EXPERIMENTAL PROCEDURES

Resource availability

Corresponding author

Further information and requests for resources and reagents should be directed to and will be fulfilled by the corresponding authors, Yoshinori Yoshida (yoshinor@cira.kyoto-u.ac.jp) and Kenji Miki (kenjimiki.prime@osaka-u.ac.jp).

Materials availability

All unique reagents generated in this study are available from the lead contact with a completed materials transfer agreement.

Data and code availability

All data are available from the corresponding authors upon request. The RNA-seq data generated in this study were deposited in the GEO database under the accession code GSE203102.

Cell culture and differentiation

Details are provided in the supplemental information. All experiments involving human iPS cells were conducted in accordance with Kyoto University Graduate School and Faculty of Medicine, Ethics Committee.

Generation of hiPSC lines harboring HCM mutants

1390D4 and 1390C1 hiPSCs were subjected to genome editing using CRISPR-Cas9. Details are provided in the supplemental information.

ECT generation and contractile force measurement

ECT generation methods were previously described (Fujiwara et al., 2021). Details are provided in the supplemental information.

Flow cytometry

Details are provided in the supplemental information.

Immunofluorescence staining and image analysis

Day-15 ECTs were used for analysis. Details are provided in the supplemental information.

DNA and RNA extraction and qPCR

Details are provided in the supplemental information.

Library preparation, RNA-seq, and bioinformatics analysis

Details are provided in the Supplementary Methods.

Western blotting

Dissociated day-29 iPSC-CMs were analyzed. Details are provided in the supplemental information.

Glucose consumption measurement

Details are provided in the supplemental information.

Statistical analysis

For comparisons between the two groups, statistical significance was determined using the unpaired two-tailed t test. For multiple comparisons, statistical significance between each group was analyzed using a one-way or two-way analysis of variance (-ANOVA) followed by Dunnett's test, Tukey's honest significant difference test, or Šídák's multiple comparisons test using GraphPad Prism9. All data were obtained from at least three independent experiments.

SUPPLEMENTAL INFORMATION

Supplemental information can be found online at https://doi.org/10.1016/j.stemcr.2023.09.003.

ACKNOWLEDGMENTS

We thank Drs. Shinya Yamanaka, Seigo Izumo, and Yasushi Kajii for supporting this project. We also thank Takako Sono, Izumi Yamada, and Shigeru Kondo for material preparation and technical assistance, and Yoko Uematsu, Kaoru Shimizu, Mikako Marx-Mori, Yumi Monnai, and Takanori Matsuo for administrative support, and Kelvin Hui for proofreading the manuscript. This work was supported by the Takeda-CiRA collaboration program and by grants from Takeda Pharmaceutical Company Limited; Japan Society for the Promotion of Science KAKENHI (20K16218, JP18K15120, JP18KK0461, and JP21H02912); Leducq Foundation (18CVD05); Research Center Network for Realization of Regenerative Medicine, AMED (JP20bm0104001, JP21bm0204003, JP21bm0804008, JP21bm0804022, and JP23bm1423011); Research on Regulatory Science of Pharmaceuticals and Medical Devices, AMED (21mk0101189, JP22mk0101241); Translational Research grant,

AMED (JP22ym0126091); Research Project for Practical Applications of Regenerative Medicine, AMED (JP21bk0104095); and the iPS Cell Research Fund and the Kyoto University Foundation.

AUTHOR CONTRIBUTIONS

Y.F., K.M., K.D., S.F., T.N., K.I., and Y.Y. conceived and designed the project. Y.F., K.M., Y.N., M.S., A.S., M.K., S.I., and T.S. performed the experimental work. Y.F., K.M., S.F., and Y.Y. wrote the manuscript. All authors discussed the results.

DECLARATION OF INTERESTS

Y.Y. and S.F. are scientific advisors of Orizuru Therapeutics, Inc. Y.Y. received research funding from Takeda Pharmaceutical Company, Ltd., and Altos Labs, Inc. Y.Y. owns stock in iPS Portal, Inc. K.D., A.S., S.I., and K.I. are employees of Takeda Pharmaceutical Company, Ltd. T.N. is an employee of Orizuru Therapeutics, Inc. T.S. is an employee of GenAhead Bio, Inc. K.M. and Y.Y. are the inventors of the patent application (WO2019/189554).

DECLARATION OF GENERATIVE AI AND AI-ASSISTED TECHNOLOGIES IN THE WRITING PROCESS

In preparing this work, the authors used ChatGPT to proofread the manuscript. After using this tool, the authors reviewed and edited the content as needed and take full responsibility for the content of this publication.

Received: October 16, 2022
Revised: September 5, 2023
Accepted: September 6, 2023
Published: October 5, 2023

REFERENCES

Authors/Task Force members, Elliott, P.M., Anastasakis, A., Borger, M.A., Borggrefe, M., Cecchi, F., Charron, P., Hagege, A.A., Lafont, A., Limongelli, G., et al. (2014). 2014 ESC Guidelines on diagnosis and management of hypertrophic cardiomyopathy: the Task Force for the Diagnosis and Management of Hypertrophic Cardiomyopathy of the European Society of Cardiology (ESC). Eur. Heart J. *35*, 2733–2779. https://doi.org/10.1093/eurheartj/ehu284.

Cohn, R., Thakar, K., Lowe, A., Ladha, F.A., Pettinato, A.M., Romano, R., Meredith, E., Chen, Y.S., Atamanuk, K., Huey, B.D., and Hinson, J.T. (2019). A Contraction Stress Model of Hypertrophic Cardiomyopathy due to Sarcomere Mutations. Stem Cell Rep. *12*, 71–83. https://doi.org/10.1016/j.stemcr.2018.11.015.

Fujiwara, Y., Deguchi, K., Miki, K., Nishimoto, T., and Yoshida, Y. (2021). A Method for Contraction Force Measurement of hiPSC-Derived Engineered Cardiac Tissues. Methods Mol. Biol. *2320*, 171–180. https://doi.org/10.1007/978-1-0716-1484-6_17.

Funakoshi, S., Fernandes, I., Mastikhina, O., Wilkinson, D., Tran, T., Dhahri, W., Mazine, A., Yang, D., Burnett, B., Lee, J., et al. (2021). Generation of mature compact ventricular cardiomyocytes from human pluripotent stem cells. Nat. Commun. *12*, 3155. https://doi.org/10.1038/s41467-021-23329-z.

Helms, A.S., Thompson, A.D., Glazier, A.A., Hafeez, N., Kabani, S., Rodriguez, J., Yob, J.M., Woolcock, H., Mazzarotto, F., Lakdawala, N.K., et al. (2020). Spatial and Functional Distribution of MYBPC3 Pathogenic Variants and Clinical Outcomes in Patients With Hypertrophic Cardiomyopathy. Circ. Genom. Precis. Med. *13*, 396–405. https://doi.org/10.1161/CIRCGEN.120.002929.

Ho, C.Y., Charron, P., Richard, P., Girolami, F., Van Spaendonck-Zwarts, K.Y., and Pinto, Y. (2015). Genetic advances in sarcomeric cardiomyopathies: state of the art. Cardiovasc. Res. *105*, 397–408. https://doi.org/10.1093/cvr/cvv025.

Karbassi, E., Fenix, A., Marchiano, S., Muraoka, N., Nakamura, K., Yang, X., and Murry, C.E. (2020). Cardiomyocyte maturation: advances in knowledge and implications for regenerative medicine. Nat. Rev. Cardiol. *17*, 341–359. https://doi.org/10.1038/s41569-019-0331-x.

Knight, W.E., Cao, Y., Lin, Y.H., Chi, C., Bai, B., Sparagna, G.C., Zhao, Y., Du, Y., Londono, P., Reisz, J.A., et al. (2021). Maturation of Pluripotent Stem Cell-Derived Cardiomyocytes Enables Modeling of Human Hypertrophic Cardiomyopathy. Stem Cell Rep. *16*, 519–533. https://doi.org/10.1016/j.stemcr.2021.01.018.

Lan, F., Lee, A.S., Liang, P., Sanchez-Freire, V., Nguyen, P.K., Wang, L., Han, L., Yen, M., Wang, Y., Sun, N., et al. (2013). Abnormal calcium handling properties underlie familial hypertrophic cardiomyopathy pathology in patient-specific induced pluripotent stem cells. Cell Stem Cell *12*, 101–113. https://doi.org/10.1016/j.stem.2012.10.010.

Leonard, A., Bertero, A., Powers, J.D., Beussman, K.M., Bhandari, S., Regnier, M., Murry, C.E., and Sniadecki, N.J. (2018). Afterload promotes maturation of human induced pluripotent stem cell derived cardiomyocytes in engineered heart tissues. J. Mol. Cell. Cardiol. *118*, 147–158. https://doi.org/10.1016/j.yjmcc.2018.03.016.

Lompre, A.M., Mercadier, J.J., Wisnewsky, C., Bouveret, P., Pantaloni, C., D'Albis, A., and Schwartz, K. (1981). Species- and age-dependent changes in the relative amounts of cardiac myosin isoenzymes in mammals. Dev. Biol. *84*, 286–290. https://doi.org/10.1016/0012-1606(81)90396-1.

Ma, Z., Huebsch, N., Koo, S., Mandegar, M.A., Siemons, B., Boggess, S., Conklin, B.R., Grigoropoulos, C.P., and Healy, K.E. (2018). Contractile deficits in engineered cardiac microtissues as a result of MYBPC3 deficiency and mechanical overload. Nat. Biomed. Eng. *2*, 955–967. https://doi.org/10.1038/s41551-018-0280-4.

Maron, B.J., Gardin, J.M., Flack, J.M., Gidding, S.S., Kurosaki, T.T., and Bild, D.E. (1995). Prevalence of hypertrophic cardiomyopathy in a general population of young adults. Echocardiographic analysis of 4111 subjects in the CARDIA Study. Coronary Artery Risk Development in (Young) Adults. Circulation *92*, 785–789. https://doi.org/10.1161/01.cir.92.4.785.

Marston, S., Copeland, O., Jacques, A., Livesey, K., Tsang, V., McKenna, W.J., Jalilzadeh, S., Carballo, S., Redwood, C., and Watkins, H. (2009). Evidence from human myectomy samples that MYBPC3 mutations cause hypertrophic cardiomyopathy through haploinsufficiency. Circ. Res. *105*, 219–222. https://doi.org/10.1161/CIRCRESAHA.109.202440.

Miki, K., Deguchi, K., Nakanishi-Koakutsu, M., Lucena-Cacace, A., Kondo, S., Fujiwara, Y., Hatani, T., Sasaki, M., Naka, Y., Okubo, C., et al. (2021). ERRgamma enhances cardiac maturation with T-tubule formation in human iPSC-derived cardiomyocytes. Nat. Commun. *12*, 3596. https://doi.org/10.1038/s41467-021-23816-3.

Milani-Nejad, N., and Janssen, P.M.L. (2014). Small and large animal models in cardiac contraction research: advantages and disadvantages. Pharmacol. Ther. *141*, 235–249. https://doi.org/10.1016/j.pharmthera.2013.10.007.

Miron, A., Lafreniere-Roula, M., Steve Fan, C.P., Armstrong, K.R., Dragulescu, A., Papaz, T., Manlhiot, C., Kaufman, B., Butts, R.J., Gardin, L., et al. (2020). A Validated Model for Sudden Cardiac Death Risk Prediction in Pediatric Hypertrophic Cardiomyopathy. Circulation *142*, 217–229. https://doi.org/10.1161/CIRCULATIONAHA.120.047235.

Mosqueira, D., Mannhardt, I., Bhagwan, J.R., Lis-Slimak, K., Katili, P., Scott, E., Hassan, M., Prondzynski, M., Harmer, S.C., Tinker, A., et al. (2018). CRISPR/Cas9 editing in human pluripotent stem cell-cardiomyocytes highlights arrhythmias, hypocontractility, and energy depletion as potential therapeutic targets for hypertrophic cardiomyopathy. Eur. Heart J. *39*, 3879–3892. https://doi.org/10.1093/eurheartj/ehy249.

Mosqueira, D., Smith, J.G.W., Bhagwan, J.R., and Denning, C. (2019). Modeling Hypertrophic Cardiomyopathy: Mechanistic Insights and Pharmacological Intervention. Trends Mol. Med. *25*, 775–790. https://doi.org/10.1016/j.molmed.2019.06.005.

Bhavsar, P.K., Dhoot, G.K., Cumming, D.V., Butler-Browne, G.S., Yacoub, M.H., and Barton, P.J. (1991). Developmental expression of troponin I isoforms in fetal human heart. FEBS Lett. *292*, 5–8. https://doi.org/10.1016/0014-5793(91)80820-s.

Piquereau, J., and Ventura-Clapier, R. (2018). Maturation of Cardiac Energy Metabolism During Perinatal Development. Front. Physiol. *9*, 959. https://doi.org/10.3389/fphys.2018.00959.

Ronaldson-Bouchard, K., Ma, S.P., Yeager, K., Chen, T., Song, L., Sirabella, D., Morikawa, K., Teles, D., Yazawa, M., and Vunjak-Novakovic, G. (2018). Advanced maturation of human cardiac tissue grown from pluripotent stem cells. Nature *556*, 239–243. https://doi.org/10.1038/s41586-018-0016-3.

Ruan, J.L., Tulloch, N.L., Razumova, M.V., Saiget, M., Muskheli, V., Pabon, L., Reinecke, H., Regnier, M., and Murry, C.E. (2016). Mechanical Stress Conditioning and Electrical Stimulation Promote Contractility and Force Maturation of Induced Pluripotent Stem Cell-Derived Human Cardiac Tissue. Circulation *134*, 1557–1567. https://doi.org/10.1161/CIRCULATIONAHA.114.014998.

Schuldt, M., Pei, J., Harakalova, M., Dorsch, L.M., Schlossarek, S., Mokry, M., Knol, J.C., Pham, T.V., Schelfhorst, T., Piersma, S.R., et al. (2021). Proteomic and Functional Studies Reveal Detyrosinated Tubulin as Treatment Target in Sarcomere Mutation-Induced Hypertrophic Cardiomyopathy. Circ. Heart Fail. *14*, e007022. https://doi.org/10.1161/CIRCHEARTFAILURE.120.007022.

Seeger, T., Shrestha, R., Lam, C.K., Chen, C., McKeithan, W.L., Lau, E., Wnorowski, A., McMullen, G., Greenhaw, M., Lee, J., et al. (2019). A Premature Termination Codon Mutation in MYBPC3 Causes Hypertrophic Cardiomyopathy via Chronic Activation of Nonsense-Mediated Decay. Circulation *139*, 799–811. https://doi.org/10.1161/CIRCULATIONAHA.118.034624.

Somura, F., Izawa, H., Iwase, M., Takeichi, Y., Ishiki, R., Nishizawa, T., Noda, A., Nagata, K., Yamada, Y., and Yokota, M. (2001). Reduced myocardial sarcoplasmic reticulum Ca(2+)-ATPase mRNA expression and biphasic force-frequency relations in patients with hypertrophic cardiomyopathy. Circulation *104*, 658–663. https://doi.org/10.1161/hc3101.093869.

Van Driest, S.L., Ackerman, M.J., Ommen, S.R., Shakur, R., Will, M.L., Nishimura, R.A., Tajik, A.J., and Gersh, B.J. (2002). Prevalence and severity of "benign" mutations in the beta-myosin heavy chain, cardiac troponin T, and alpha-tropomyosin genes in hypertrophic cardiomyopathy. Circulation *106*, 3085–3090. https://doi.org/10.1161/01.cir.0000042675.59901.14.

Yu, G., Wang, L.G., Yan, G.R., and He, Q.Y. (2015). DOSE: an R/Bioconductor package for disease ontology semantic and enrichment analysis. Bioinformatics *31*, 608–609. https://doi.org/10.1093/bioinformatics/btu684.